Synthesis of large-scale 2-D MoS$_2$ atomic layers by hydrogen-free and promoter-free chemical vapor deposition

Hung Nguyen [a], Chih-Fang Huang [b], Weijun Luo [c], Guangrui (Maggie) Xia [c], Zhiqiang Chen [d], Zhiqiang Li [e], Christopher Raymond [e], David Doyle [e], Feng Zhao [a,*]

[a] Electrical Engineering, School of Engineering and Computer Science, Washington State University, Vancouver, WA 98686, USA
[b] Electrical Engineering, National Tsing Hua University, Hsinchu 30013, Taiwan, ROC
[c] Materials Engineering, University of British Columbia, Vancouver, B.C., Canada V6T 1Z4
[d] Center for Electron Microscopy and Nanofabrication, Portland State University, Portland, OR 97207, USA
[e] Nanometrics, 1320 SE Armour Dr, Suite B2, Bend, OR 97702, USA

ARTICLE INFO

ABSTRACT

As one of the two-dimensional (2-D) transition metal dichalcogenides, atomically thin molybdenum disulfide (MoS$_2$) has attracted significant attention and research interests for micro and nanoelectronic applications. Significant efforts have been made to develop different approaches in order to obtain atomic layer MoS$_2$, such as exfoliation, chemical synthesis, and physical or chemical vapor deposition (CVD) processes. In this paper, we report a hydrogen-free and promoter-free CVD growth to synthesize large-area MoS$_2$ atomic layers. A variety of techniques including optical microscopy (OM), atomic force microscopy (AFM), photoluminescence (PL) mapping, Raman and x-ray photoelectron spectroscopy (XPS), high resolution electron microscopy (HREM) and scanning transmission electron microscopy (STEM) were applied to characterize the film quality, uniformity and layer numbers. High quality centimeter-sized MoS$_2$ atomic layers were demonstrated, which form a foundation to develop wafer-sized material platform for device fabrication and production.

1. Introduction

Atomically thin MoS$_2$, as one of the prototypes of 2-D transition metal dichalcogenides (TMDs), has demonstrated desirable material properties for low power electronics and optoelectronic applications. These properties include large direct bandgap energy for monolayers [1,2], high carrier mobility [3], excellent current on/off ratio [4], high mechanical strength [5] and flexibility [6], etc. Considerable research efforts and investigation have been motivated to develop techniques to produce MoS$_2$ atomic layers. These techniques include various exfoliation processes [7–10], physical vapor deposition (PVD) [11–13], and chemical vapor deposition (CVD). For example, direct sulfurization of pre-deposited molybdenum thin film [14] or molybdenum trioxide (MoO$_3$) powder with graphene-like promoters [15] were reported, with MoS$_2$ crystal shapes investigated under different growth conditions [16]. A two-step thermal process [17] to convert MoO$_3$ to MoS$_2$ by hydrogen annealing and sulfurization have been demonstrated. A

self-limiting CVD approach [18] to grow MoS$_2$ films with layer numbers precisely controlled over an area of centimeters was also developed by sulfurization of MoCl$_5$. And another layer control approach for large-area MoS$_2$ film was proposed by treatment of the substrate surface with oxygen plasma [19]. Process using magnetron sputtering [20] was also developed to grow MoS$_2$ films by sputtering Mo metal target in vaporized sulfur ambient atomic high temperatures (> 700 °C). In summary, the goal of all these processes is to grow high quality large-area MoS$_2$ film, which is required for large-scale production of practical devices.

In this paper, we report a CVD synthesis method, hydrogen-free and promoter-free, for MoS$_2$ film growth on SiO$_2$/Si substrate. The film thickness, crystalline quality and layer numbers were characterized comprehensively by a variety of spectroscopic and microscopic techniques including OM, AFM, PL, Raman, XPS, HREM and STEM. Our results show that large-area MoS$_2$ atomic films were attainable with high quality as by other growth techniques, which is favorable for device applications.

* Corresponding author.
    E-mail address: feng.zhao@wsu.edu (F. Zhao).

2. Experimental

Prior to the CVD process, the SiO_2/Si substrate (SiO_2 thickness: 280 nm) was cleaned with acetone, Isopropyl Alcohol (IPA) and deionized (DI) water, followed by piranha solution (H_2SO_4:

$H_2O_2 = 1:1$) and rinse thoroughly by DI water again. After dried completely, the substrate was loaded in a 2-inch-diameter quartz tube furnace. Fig. 1(a) illustrates the CVD setup for MoS_2 growth. Solid powders of MoO_3 (99.995%, 50 mg) and S (99.999%, 50 mg) were used as the precursor materials, and high purity argon (Ar) as the carrier gas. An alumina boat was used to contain S and placed upstream relative to the Ar gas flow direction, while another boat containing MoO_3 was placed close to the center of the heating zone. At room temperature, the quartz tube was first pumped down to remove the oxygen, followed by constant Ar gas flow started with a 500 sccm rate. While the furnace was heated up with a heating rate of 10 °C/min, the Ar gas flow was adjusted as shown in Fig. 1(b) to 100 sccm when temperature reached 700 °C. The precursor MoO_3 and S reacted at 700 °C for 15 min to produce MoS_2 spices which precipitated onto the SiO_2/Si substrate to form MoS_2 thin film. After chemical synthesis, the furnace tube was cooled down to room temperature to unload the substrate.

Fig. 1. (a) Schematic diagram of the CVD system for MoS_2 atomic layer growth; (b) temperature and gas flow programming during the chemical synthesis.

3. Results and discussion

Optical characterizations of synthesized MoS_2 atomic film on the SiO_2/Si substrate are shown in Fig. 2. Photograph in Fig. 2 (a) displays the color of the as-grown MoS_2 under white light. Color contrast clearly shows areas of MoS_2 and SiO_2. Magnified image of MoS_2 film taken under optical microscope is illustrated in Fig. 2(b). It can be seen that the film is uniform and continuous across a large area without grain boundary. The thickness of the MoS_2 film was measured by AFM. Fig. 2(c) shows a typical AFM image of triangle-shaped MoS_2 crystals with clear grain boundaries attained by our CVD growth. Such triangle shape was also
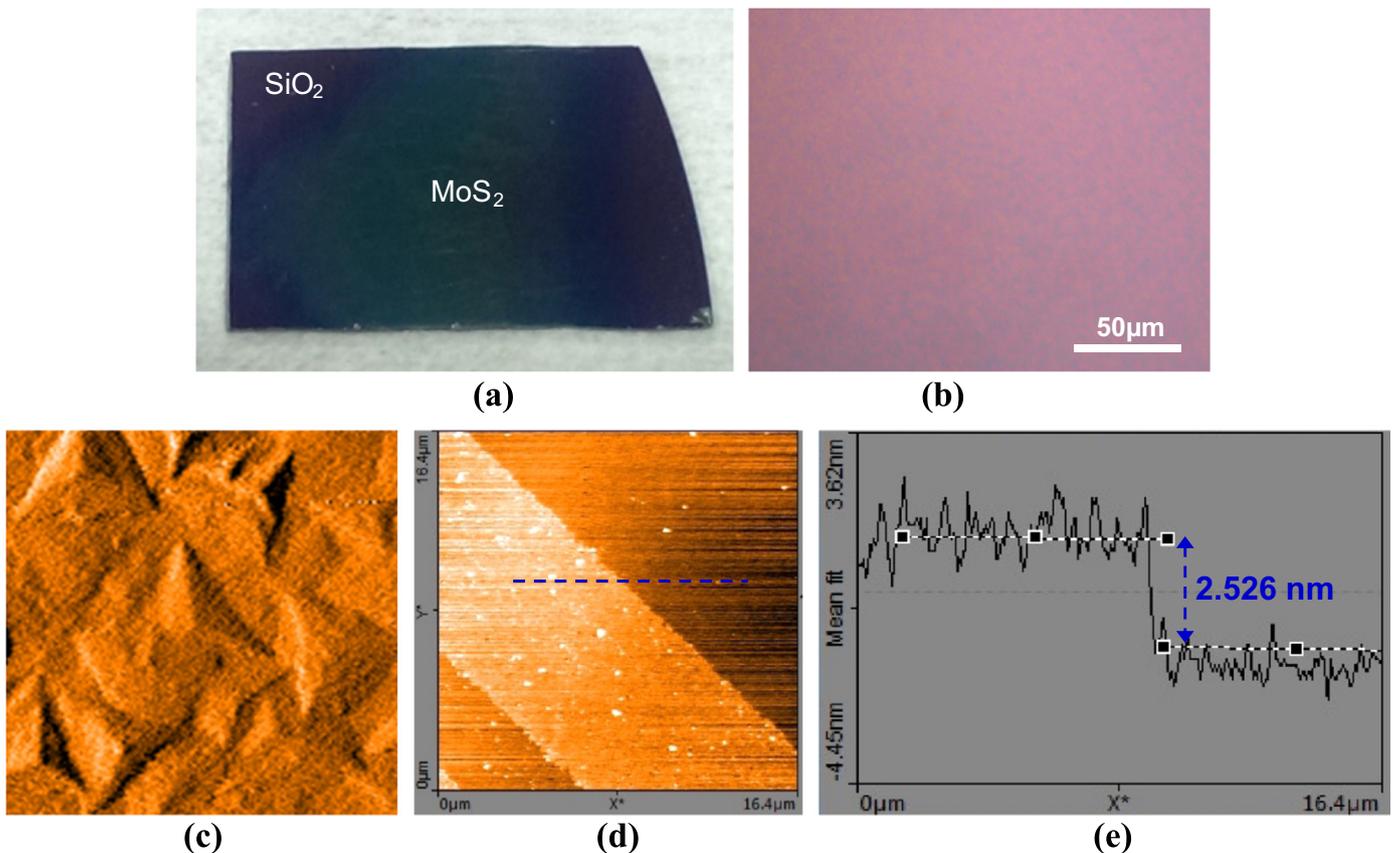
Fig. 2. Synthesized MoS_2 film on a SiO_2/Si substrate with (a) optical photograph with clear color contrast between MoS_2 and SiO_2, (b) microscopic image of MoS_2 film, and AFM images of MoS_2 crystals (c) in triangle shape before growth improvement, (d) forming a continuous film after improvement of growth parameters, and (e) thickness profile of a tri-layer MoS_2 film.
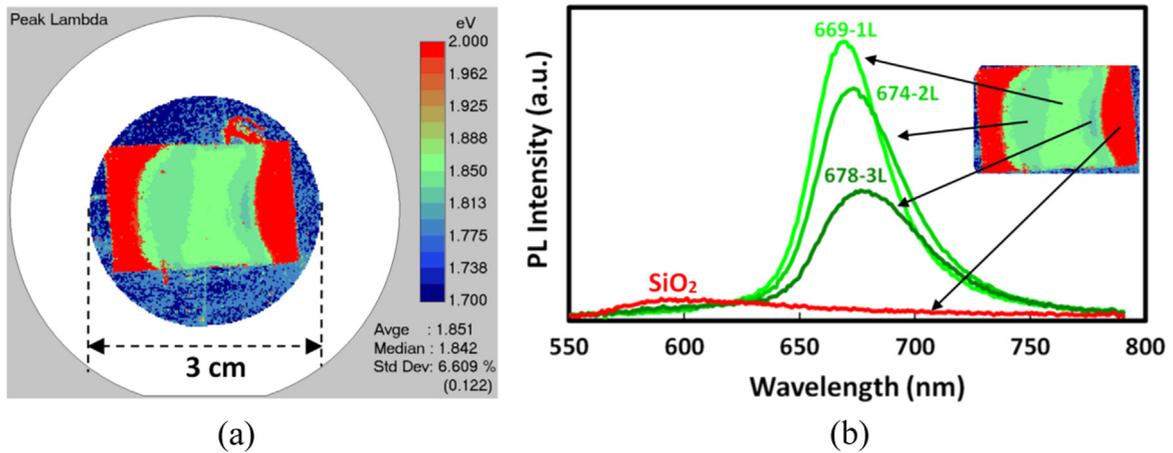
Fig. 3. PL characterization of synthesized MoS_2 films grown on a SiO_2/Si substrate. (a) PL mapping with a scanning spatial resolution of 200 μm × 200 μm across the substrate. (b) PL spectra from 4 different areas on the substrate showing layer numbers and thickness dependence of the PL intensity.
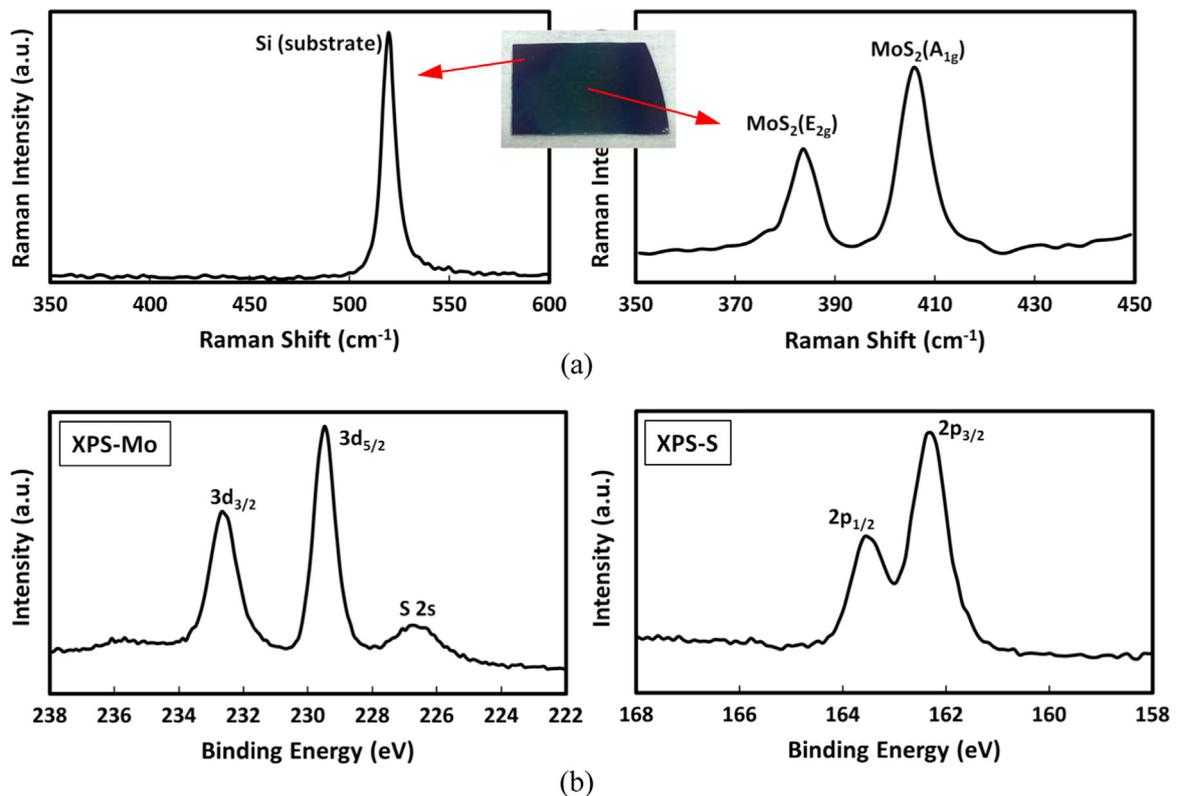
Fig. 4. (a) Raman spectra of Si substrate and synthesized tri-layer MoS_2 on the substrate with two peaks positioned at 383.6 cm^{-1} and 405.7 cm^{-1}, corresponding to the E_{2g} and A_{1g} vibration modes, respectively. (b) XPS scan of the synthesized MoS_2 film with binding energy of Mo 3d at 229.5 eV and 232.6 eV, and S 2p at 162.3 eV and 163.6 eV.

reported by other publications, for example, [15,16]. With improvement of growth conditions, these crystals now form a continuous form as shown in Fig. 2(d). A scratch was made intentionally for AFM scanning. The height profile of a tri-layer MoS_2 film with a thickness of 2.526 nm is shown in Fig. 2(e). The image also confirms the absence of grain boundary in micrometer scale.

PL was performed by a commercial room temperature PL mapping system, VerteX from Nanometrics, Inc., to characterize and confirm the synthesized MoS_2 atomic layers. A diode-pumped solid-state laser (532 nm, 50 mW) was applied as the excitation source to scan an area of 3 cm-diameter which covers the whole SiO_2/Si substrate, with a scanning spatial resolution of 200 μm × 200 μm. The mapping of λ_{peak} across the whole substrate is shown in Fig. 3(a) using the software equipped in the VerteX system. Typical PL spectra collected from 4 different areas (different

colors as in Fig. 3(a)) on the SiO_2/Si substrate are illustrated in Fig. 3 (b) with signal intensity normalized. These peaks in the PL spectra are around ~670 nm (1.85 eV), which is correlated to the A direct excitonic transition of MoS_2. It can be also seen that the PL spectrum of the monolayer MoS_2 film shows the strongest emission, and the intensity drops for bilayer and tri-layer films. This confirms that the optical property of as-grown MoS_2 films exhibit dependence on layer numbers due to an evolution of the bandgap with the layer no. This result is similar as the exfoliated films and synthesized films reported by other methods [18,20–22]. It is noted that the PL peak corresponding to the B exciton is not clear, which is usually attributed to lattice disorder or residual dopants that decouple the spin–orbital interaction [20,23].

Raman and XPS spectroscopy was applied to further confirm and evaluate the quality of synthesized MoS_2 films. A LabRAM HR
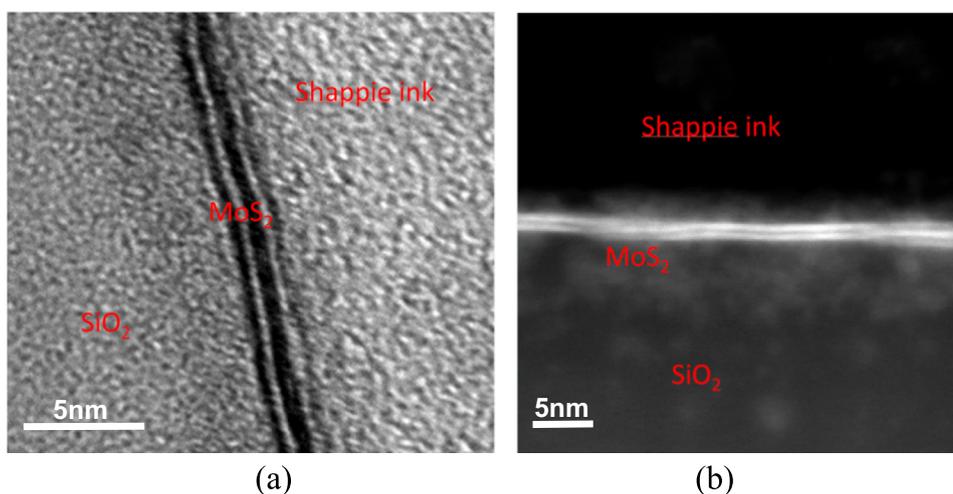
Fig. 5. (a) HREM and (b) STEM Z contrast images show the synthesized monolayer and bilayer MoS$_2$ films.

Raman confocal microscope by Horiba Scientific was used for measurement. The wavelength of the input laser was 442 nm. Fig. 4(a) shows a representative characteristic in comparison of signals from areas with and without MoS$_2$ film. The area without MoS$_2$ only shows the peak of Si substrate which is at 520.6 cm^{-1}. The area with MoS$_2$ shows two peaks of 383.6 cm^{-1} and 405.7 cm^{-1}, which correspond to the E_{2g} and A_{1g} vibration modes, respectively. It has been reported that the separation ($\Delta = A_{1g} - E_{2g}$) between these two Raman peaks relates to the no of MoS$_2$ layers [24]. In this area under test, $\Delta = 22$ cm^{-1}, which indicates bilayer [18] MoS$_2$ crystals in this area. Chemical configuration of the synthesized MoS$_2$ film was analyzed and confirmed by XPS characterization. Fig. 4(b) shows the XPS spectra of as-grown MoS$_2$ film for Mo 3d and S 2p. Mo 3d spectra peaks at two binding energies of 229.5 eV and 232.6 eV, which are attributed to 3d$_{5/2}$ and 3d$_{3/2}$ of Mo^{6+}. S 2p also exhibits two characteristic peak positions at binding energies of 162.3 eV and 163.6 eV, corresponding to spin–orbit 2p$_{3/2}$ and 2p$_{1/2}$, respectively. All these peak positions are in close agreement with other reported values [15,25], and confirm that the synthesized MoS$_2$ film have 2h-MoS$_2$ crystal structure with semiconductor properties [2,26].

HREM and STEM characterizations were applied to further elucidate the MoS$_2$ film and layer numbers. Regular TEM cross-section samples were prepared with a FEI Strata 237 FIB. Prior to FIB milling, a thin layer of Shappie was applied to specimen surface to prevent ion beam damage. HREM and STEM Z contrast images were taken in a FEI TECNAI F20 supertwin TEM with a Fischione high angle annular dark field detector (HAADF). Some representative images are displayed in Fig. 5. As observed in Fig. 5 (a), bilayer MoS$_2$ film is shown in this local area, which is consistent with the STEM Z contrast image in Fig. 5(b) by the two bright lines. These layer numbers are in agreement with the results from our AFM, Raman and PL measurements. Such clear two-layer structure also confirms the crystalline nature of the as-grown MoS$_2$ material.

4. Summary

In this paper we presented preparation of high quality and large area MoS$_2$ at crystals by CVD process. Monolayer and few-layered MoS$_2$ films were synthesized on a centimeter-sized SiO$_2$/Si substrate. The size and uniformity of the films, the thickness and layer numbers, crystal quality, optical property and chemical configurations were characterized by a variety of techniques. The results confirm that it is promising to grow wafer scale MoS$_2$ film to realize its applications in electronics.

References

[1] K.F. Mak, C. Lee, J. Hone, J. Shan, T.F. Heinz, Phys. Rev. Lett. 105 (2010) 136805.
[2] C. Ataca, H. Sahin, S. Ciraci, J. Phys. Chem. C 116 (2012) 8983–8999.
[3] B. Radisavljevic, A. Radenovic, J. Brivio, B. Giacometti, A. Kis, Nat. Nanotechnol. 6 (2011) 147–150.
[4] W. Wu, D. De, S.C. Chang, Y.N. Wang, H.B. Peng, J.M. Bao, et al., Appl. Phys. Lett. 102 (2013) 142106.
[5] Q. Peng, S. De, Phys. Chem. Chem. Phys. 15 (2013) 19427–19437.
[6] Y. Yang, H.L. Fei, G.D. Ruan, C.S. Xiang, J.M. Tour, Adv. Mater. 26 (2014) 8163–8168.
[7] N. Liu, P. Kim, J.H. Kim, J.H. Ye, S.K. Kim, C.J. Lee, ACS Nano 8 (2014) 6902–6910.
[8] H. Li, J. Wu, Z.Y. Yin, H. Zhang, Accounts Chem. Res. 47 (2014) 1067–1075.
[9] E. Varrla, C. Backes, K.R. Paton, A. Harvey, Z. Gholamvand, J. McCauley, et al., Chem. Mater. 27 (2015) 1129–1139.
[10] L. Dong, S. Lin, L. Yang, J.J. Zhang, C. Yang, D. Yang, et al., Chem. Commun. 50 (2014) 15936–15939.
[11] C. Muratore, J.J. Hu, B. Wang, M.A. Haque, J.E. Bultman, M.L. Jespersen, et al., Appl. Phys. Lett. 104 (2014) 261604.
[12] S. Helveg, J.V. Lauritsen, E. Lægsgaard, I. Stensgaard, J.K. Nørskov, B.S. Clausen, et al., Phys. Rev. Lett. 84 (2000) 951–954.
[13] J.V. Lauritsen, J. Kibsgaard, S. Helveg, H. Topsøe, B.S. Clausen, E. Lægsgaard, et al., Nat. Nanotechnol. 2 (2007) 53–58.
[14] Y. Zhan, Z. Liu, S. Najmaei, P.M. Ajayan, L. Lou, Small 8 (2012) 966–971.
[15] Y.H. Lee, X.Q. Zhang, W. Zhang, M.T. Chang, C.T. Lin, K.D. Chang, et al., Adv. Mater. 24 (2012) 2320–2325.
[16] S. Wang, Y.M. Rong, Y. Fan, M. Pacios, H. Bhaskaran, K. He, et al., Chem. Mater. 26 (2014) 6371–6379.
[17] Y.C. Lin, W.J. Zhang, J.K. Huang, K.K. Liu, Y.H. Lee, C.T. Liang, et al., Nanoscale 4 (2012) 6637–6641.
[18] Y.F. Yu, C. Li, Y. Liu, L.Q. Su, Y. Zhang, L.Y. Cao, Sci. Rep. 3 (2013) 1866.
[19] J. Jeon, S.K. Jang, S.M. Jeon, G. Yoo, Y.H. Jang, J.H. Park, et al., Nanoscale 7 (2015) 1688–1695.
[20] J.G. Tao, J.W. Chai, X. Lu, L.M. Wong, T.I. Wong, J.S. Pan, et al., Nanoscale 7 (2015) 2497–2503.
[21] K.K. Liu, W. Zhang, Y.H. Lee, Y.C. Lin, M.T. Chang, C. Su, Nano Lett. 12 (2012) 1538–1544.
[22] Y. Lee, J. Lee, H. Bark, I.K. Oh, G.H. Ryu, Z. Lee, Nanoscale 6 (2014) 2821–2826.
[23] A.P.S. Gaur, S. Sahoo, M. Ahmadi, S.P. Dash, M.J.F. Guinel, R.S. Katiyar, Nano Lett. 14 (2014) 4314–4321.
[24] C. Lee, H. Yan, L.E. Brus, T.F. Heinz, J. Hone, S. Ryu, ACS Nano 4 (2010) 2695–2700.
[25] N.H. Turner, A.M. Single, Surf. Interface Anal. 15 (1990) 215–222.
[26] C.A. Papageorgopoulos, W. Jaegermann, Surf. Sci. 338 (1995) 83–93.